doi.org/10.1002/cbdv.202301227 Research Article CHEMISTRY & BIODIVERSITY

www.cb.wiley.com

Computational Screening of Neuropilin-1 Unveils Novel Potential Anti-SARS-CoV-2 Therapeutics

Michael Afiadenyo,*[a] Latif Adams,*[b, f] Clement Agoni,[c, d, e] Siobhan Moane,[b] Michelle Mckeon-Bennett,[b] Dorcas Obiri-Yeboah,[f] and Jasdeep Singh[g]

Neuropilin 1 (NRP-1) inhibition has shown promise in reducing the infectivity of severe acute respiratory syndrome-coronavirus-2 (SARS-CoV-2) and preventing the virus entry into nerve tissues, thereby mitigating neurological symptoms in COVID-19 patients. In this study, we employed virtual screening, including molecular docking, Molecular Dynamics (MD) simulation, and Molecular Mechanics-Poisson Boltzmann Surface Area (MM-PBSA) calculations, to identify potential NRP-1 inhibitors. From a compendium of 1930 drug-like natural compounds, we identified five potential leads: CNP0435132, CNP0435311, CNP0424372, CNP0429647, and CNP0427474, displaying robust binding energies of −8.2, −8.1, −10.7, −8.2, and −8.2 kcal/mol, respectively. These compounds demonstrated interactions with critical residues Tyr297, Trp301, Thr316, Asp320, Ser346, Thr349, and Tyr353 located within the b1 subdomain of NRP-1. Furthermore, MD simulations and MM-PBSA calculations affirmed the stability of the complexes formed, with average root mean square deviation, radius of gyration, and solvent accessible surface area values of 0.118 nm, 1.516 nm, and 88.667 nm^2, respectively. Notably, these lead compounds were estimated to penetrate the blood-brain barrier and displayed antiviral properties, with Pa values ranging from 0.414 to 0.779. The antagonistic effects of these lead compounds merit further investigation, as they hold the potential to serve as foundational scaffolds for the development of innovative therapeutics aimed at reducing the neuroinfectivity of SARS-CoV-2.

Introduction

Severe Acute Respiratory Syndrome Coronavirus-2 (SARS-CoV-2) is the virus liable for the disease COVID-19.[1,2] The virus spreads through the aerosols of infected persons upon coughing or sneezing.[2,3] About 300 million confirmed cases have been recorded with more than 5 million deaths as of 2023.[4] Symptoms shown by infected persons include, fever, cough, pneumonia, loss of taste, loss of smell, diarrhea, hemoptysis, and fatigue.[1,3,5] COVID-19 has also shown to be a systematic disease, affecting the central nervous system.[6,7] Symptoms such as depression, anxiety, and loss of smell and taste are associated with the nervous system.[8] SARS-CoV-2 infectivity and neuronal expression of ACE2 are only found in human pluripotent stem cells (PSCs)-derived mixed neurons or human brain organoids, not in human brain tissue.[9] Earlier studies have suggested that the olfactory route and the brain-blood barrier (BBB) are plausible routes utilized by SARS-CoV-2 to get access to the nerve tissues and the brain.[9,10]

Neuropilin-1 (NRP-1) has been identified as the receptor that promotes the entry of SARS-CoV-2 into the nerve tissues and the brain through the hematogenous route (permeating the BBB) and the olfactory nerve.[9,10] This accounts for the expression of the virion's protein in the brain of some deceased COVID-19 patients while some living patients exhibit neurological symptoms.[9,11–15]

Neuropilins are cell surface proteins that are widely distributed and participate in a variety of vital cellular signaling cascades.[16,17] There are two families of Neuropilins namely, Neuropilin-1 (NRP-1) and Neuropilin-2 (NRP-2).[18,19] Both are transmembrane proteins with a cytosolic C terminus and an extracellular N terminus.[20] At the amino acid level, NRP-1 and NRP-2 have about 44% identity.[16,21] Neuropilins have three domains namely, extracellular, transmembrane, and cytosolic domains. Within the extracellular domain lie three subdomains namely, A (a1-a2), B (b1-b2), and C.[20]

Neuropilins have a high affinity to Vascular Endothelial Growth Factor (VEGF) and class 3 semaphorins (Sema3).[22] Due to their ubiquitous nature, Neuropilins play a critical role in the

[a] M. Afiadenyo
Department of Parasitology, Noguchi Memorial Institute for Medical Research
College of Health Sciences, University of Ghana, Legon, Accra, Ghana
E-mail: afiadenyom755@gmail.com

[b] L. Adams, S. Moane, M. Mckeon-Bennett
Technological University of Shannon: Midlands Midwest
Midlands Campus, Athlone, Ireland
E-mail: latifadams2016@yahoo.com
Abdullatif.adams@tus.ie

[c] C. Agoni
UCD Conway Institute of Biomolecular and Biomedical Research
School of Medicine, University College Dublin, Belfield D04, V1 W8, Ireland

[d] C. Agoni
Discipline of Pharmaceutical Sciences, School of Health Sciences
University of KwaZulu-Natal, Westville Campus, Durban 4001, South Africa

[e] C. Agoni
West African Centre for Computational Research and Innovation, Ghana

[f] L. Adams, D. Obiri-Yeboah
Department of Microbiology and Immunology, School of Medical Sciences
College of Health and Allied Sciences, University of Cape Coast, Cape Coast, Ghana

[g] J. Singh
Department of Biochemical Engineering and Biotechnology
Indian Institute of Technology-Delhi, New Delhi, Delhi, India

Supporting information for this article is available on the WWW under https://doi.org/10.1002/cbdv.202301227

cardiovascular and nervous systems.[22,23] The B (b1-b2) subdomain of the extracellular domain has a core role in specific ligand binding and competition for many ligands.[16]

SARS-CoV-2 expresses both structural and non-structural proteins including the spike, envelope, membrane and nucleocapsid proteins.[24] The spike protein binds to a receptor and facilitates viral cell invasion. Proteases like Transmembrane Protease Serine 2 (TMPRSS2) and furin activate the spike protein during the attachment and cell invasion process.[25,26] The spike protein is made up of 2 units namely S1 and S2. Furin cleaves the spike protein at the S1/S2 site while TMPRSS2 cleaves at the S2 site.[27] The Receptor Binding Domain (RDB), N-Terminus Domain (NTD), and C-Terminus Domain (CTD) make up the S1 unit.[25] At the CTD of the S1 unit, is a C-end Rule (RRAR) after the activation of the spike protein by furin.[11,28] Due to the b1 subdomain's high affinity to ligands,[29] the C-end Rule binds to the b1 subdomain of NRP-1 to enhance cell entry (Figure 1). The C-end Rule interacts with residues Tyr297, Trp301, Thr316, Asp320, Ser346, Ther349 and Tyr353.[11,12,28] Previous studies have also shown that Trp411, Lys351 and Ser348 are critical residues in the activity of NRP-1[30] (Figure 2). It is therefore imperative to identify small molecules that can interrupt the interaction between the b1 subdomain and the C-end Rule.[31]

Natural products are chemical compounds that are attained from living things and can be used as drugs due to their bioactivity.[32] Over the years, natural compounds have served as a hub for drugs and clinical pharmaceuticals utilize natural products for drugs as about 50% of natural products do not violate Lipinski's rule of five (Ro5) for orally available drugs.[32,33] This study aimed to identify novel natural compounds that are plausible inhibitors of NRP-1 via molecular docking, MD simulation, and MM-PBSA calculations.

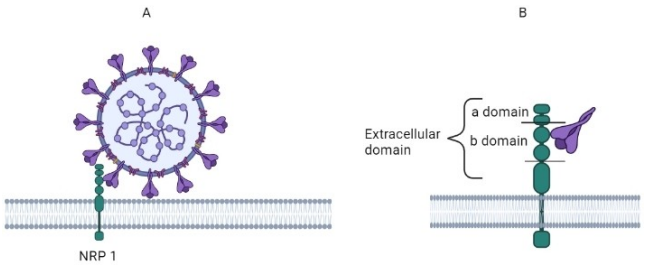

Figure 1. The interaction between the (A) spike protein and NRP-1 enabling the SARS-CoV-2 virus get access to the nervous system. (B) The C-end Rule interacts with the b1 subdomain of NRP-1.

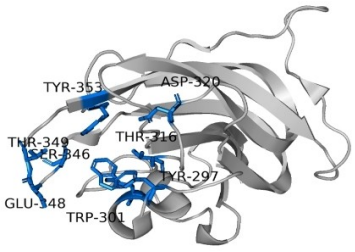

Figure 2. The structure of NRP-1 showing the active sites (blue) involved in the interaction between NRP-1 and the C-end Rule. The active sites constitute the residue lining of the b1 subdomain.

Results and Discussion

Virtual screening of small molecules against a desired target is crucial in computer-aided drug design. This is to identify molecules that bind to a target with high affinity and specificity.[34] A total of 1930 compounds were virtually screened against the b1 subdomain of NRP-1 to identify potential inhibitors. Protein-ligand interaction, MD simulation, and MM-PBSA calculations were computed to gain insight into the mechanism of binding and the stability of the NRP-1-potential lead complexes.[35]

Molecular docking

A compendium of 1930 compounds, two inhibitors and the C-end Rule were virtually screened against the b1 subdomain of NRP-1. The binding energies between the C-end Rule, EG00229, and EG01377 and NRP-1 were −6.4, −6.5 and −6.6 kcal/mol respectively. These results corroborate previous studies where among the three, the C-end Rule had the least binding affinity followed by EG00229 and finally EG01377.[36–38] −7.0 kcal/mol has been used as a threshold for choosing potential antiviral compounds and has also conjointly been shown to tell apart between putative and non-putative target binders.[39–41] Furthermore, a threshold of −7.23 kcal/mol was utilized in a previous study where NRP-1 inhibitors were identified[42] hence, a stringent threshold of −8.0 kcal/mol was adopted. A total of 34 hits with binding energies less than −8.0 kcal/mol were selected. Among the 34 hits was CNP0426052 with the strongest binding affinity of −11.9 kcal/mol (Table 1).

Assessment of docking protocol

Assessment of docking protocol is important in determining the performance and efficiency of AutoDock Vina. LigAlign[43] script embedded in PyMOL version 1.3 was employed. LigAlign employs the superposition of ligands in validating the docking protocol by determining the root mean square deviation (RMSD) between the co-crystallized and the redocked ligands. This technique is widely adopted for structural analysis of the protein-ligand complex.[44] An RMSD value of 1.660 Å was obtained. An RMSD value less than or equal to 2.0 Å depicts AutoDock Vina's ability to predict the binding pose of the ligand in the binding pocket.[43,45]

After the superposition of the co-crystallized and the re-docked structures, 10 residues interact with the C-end rule with 4 being hydrogen bonds and 6 being hydrophobic interactions. 7 out of the 10 residues are the critical residues Tyr297, Trp301, Thr316, Asp320, Ser346, Thr349 and Tyr353. Asp320, Tyr353, Thr349 and Ser346 formed hydrogen bonds while Tyr297, Trp301 and Thr316 formed hydrophobic interactions (Figure 3).

Table 1. The binding energy and protein-ligand interaction of compounds with binding energy of ≥-7.5 kcal/mol that formed at least a hydrogen bond.

Compound	Binding Energy [kcal/mol]	Hydrogen Bond Length [Å]	Hydrophobic Interactions
CNP0426052	−11.9	Trp301(3.11)	Tyr297, Asp320, Thr316, Tyr353
CNP0435138	−11.4	Trp301 (3.15)	Tyr297, Thr316, Tyr353
CNP0427275	−11.4	Asp320 (3.08)	Thr316, Trp301, Tyr353, Tyr297
CNP0425170	−11.1	Ile345 (2.97)	Arg418, Lys347, Ser346
CNP0425047	−10.9	Pro311 (3.10), Ile345 (2.94)	Thr388, Arg418, Lys347, Ser346
CNP0426390	−10.9	Thr316 (2.84), Ile415 (3.23)	Gly414, Tyr353, Tyr297, Trp301
CNP0424372	−10.7	Asp320(3.09,3.14)	Gly414, Tyr297, Thr316, Tyr353, Trp301
CNP0426601	−8.9	Ile415 (3.22), Asp320 (3.13)	Thr316, Tyr353, Trp301, Tyr297, Gly414
CNP0428817	−8.5	Trp301 (2.87)	Tyr297, Lys351, Thr316, Thr413, Asp320, Tyr353, Thr349
CNP0431473	−8.4	Asp320 (3.01), Pro317 (3.25)	Gly318, Thr316, Tyr353, Glu348, Ser346, Trp301, Tyr297, Glu319
CNP0436773	−8.3	Tyr297 (3.00), Ser346 (3.17) Tyr353 (2.80, 3.17)	Asn300, Thr349, Glu348, Trp301, Asp320, Thr316, Glu319, Gly318
CNP0433083	−8.3	Tyr353 (2.83), Trp301 (2.88)	Thr349, Glu348, Tyr297, Thr316, Glu319, Asp320
CNP0435132	−8.2	Asp320 (3.06)	Glu319, Pro317, Thr316, Trp301, Tyr297, Tyr353
CNP0429647	−8.2	Trp301 (3.12)	Tyr297, Gly414, Thr316, Asp320, Tyr353, Thr413, Thr349, Glu348
CNP0427474	−8.2	Asp320 (3.07), Ser346 (3.03), Glu348 (2.91)	Thr316, Tyr297, Trp301, Tyr353
CNP04432501	−8.2	Asp320 (2.97), Ser346 (3.33), Trp301 (3.05)	Gly414, Tyr353, Thr316, Glu348, Thr349, Tyr297
CNP0434819	−8.2	Asp320 (3.07), Ser346 (3.03), Glu348 (2.91)	Thr316, Tyr297, Tyr353, Trp301
CNP0435311	−8.1	Trp301 (2.98)	Glu348, Thr349, Asp320, Thr316, Tyr353, Tyr297
CNP0429190	−8	Trp301 (3.23), Asp320 (3.04), Thr413 (3.00)	Thr349, Glu348, Tyr297, Thr316, Tyr353, Gly414
CNP0430366	−8	Tyr353 (3.16), Thr349 (3.04), Asp320 (2.80)	Glu319, Thr316, Ser346, Trp301, Tyr297, Glu348
CNP0435892	−7.9	Tyr353 (2.99)	Trp301, Tyr297, Lys351, Glu319, Asp320, Thr316
CNP0434791	−7.9	Trp301 (2.81)	Thr316, Tyr353, Gly414, Asp320, Tyr297
CNP0429699	−7.9	Asp320 (3.04)	Ser346, Tyr353, Glu319, Pro317, Thr316, Tyr297, Trp301, Thr349
CNP0433536	−7.9	Ser346 (3.29), Glu348 (3.30), Trp301 (3.14)	Tyr353, Thr316, Asp320, Tyr297, Thr349
CNP0432708	−7.9	Ser346 (3.30), Glu348 (3.20), Trp301 (3.01)	Thr316, Asp320, Tyr353, Tyr297
CNP0434613	−7.9	Asp320 (2.89), Trp301 (3.02)	Tyr297, Thr316, Tyr353
CNP0433856	−7.9	Asp320 (3.00), Trp301 (3.14), Ser346 (3.21)	Thr316, Gly414, Tyr297, Tyr353, Thr349
CNP0434111	−7.9	Trp301 (3.28)	Glu348, Tyr297, Asp320, Pro317, Thr316, Tyr353
CNP0430421	−7.9	Asp320 (3.12), Trp301 (3.10)	Pro317, Glu319, Tyr297, Thr316, Thr349, Ser346
CNP0425385	−7.9	Tyr353 (3.18), Glu348 (3.00), Asn300 (3.14,2.80), Ser298 (3.10)	Asp320, Gly414, Thr316, Thr349, Trp301, Tyr297
CNP0425875	−7.9	Ser346 (2.77, 2.98), Glu348 (3.03), Thr349 (3.24), Tyr353 (2.96, 3.15)	Trp301, Tyr297, Thr316
CNP0426315	−7.8	Asp320 (3.25)	Thr316, Trp301, Tyr353, Thr349, Ser346, Tyr297, Glu319
CNP0433097	−7.8	Asp320 (3.19)	Pro317, Thr316, Tyr297, Trp301, Ser346, Tyr353, Lys351, Glu319
CNP0432892	−7.8	Tyr353 (3.13), Ser346 (3.11, 2.97), Glu348 (3.03)	Thr349, Trp301, Tyr297, Thr316, Asp320, Glu319
CNP0430138	−7.8	Try353 (3.17), Trp301 (3.18, 2.93)	Thr316, Tyr297, Thr349
CNP0433268	−7.8	Asp320 (3.22), Asn300 (3.30)	Glu319, Thr349, Glu348, Tyr297, Trp301, Tyr353, Thr316
CNP0425897	−7.8	Trp301 (3.29)	Asp320, Tyr297, Thr349, Thr316
CNP0435506	−7.8	Ser346 (2.88)	Thr349, Trp301, Tyr297, Tyr353, Pro317, Thr316, Asp320, Glu319, Glu348
CNP0424610	−7.8	Tyr353 (2.86), Thr413 (2.88, 2.92), Asp320 (3.00)	Gly414, Thr316, Tyr297, Trp301, Thr349, Lys351, Glu348
CNP0424533	−7.8	Asp320 (3.16, 3.32)	Glu319, THR316, Trp301, Tyr297
CNP0425464	−7.8	Tyr353 (2.81), Trp301 (3.10)	Asp320, Thr413, Thr316, Gly414, Tyr297, Lys351, Asn300, Glu348
CNP0432611	−7.8	Ser346 (3.21), Trp301 (3.12)	Thr349, Glu348, Tyr297, Tyr353, Asp320, Thr316
CNP0429474	−7.8	Lys351 (3.33)	Thr413, Asp320, Tyr353, Tyr297, Trp301
CNP0433023	−7.8	Glu348 (2.87), Ser346 (3.20)	Thr349, Lys351, Tyr353, Thr316, Asp320, Gly318, Glu319, Tyr297, Trp301

Table 1. continued

Compound	Binding Energy [kcal/mol]	Hydrogen Bond Length [Å]	Hydrophobic Interactions
CNP0424522	−7.8	Lys351 (3.21), Asp320 (2.98)	Glu319, Thr316, Trp301, Tyr297, Tyr353
CNP0431265	−7.8	Asn300 (3.20), Trp301 (3.21, 2.87)	Tyr297, Tyr353, Thr316, Glu348
CNP0427137	−7.7	Asp320 (3.02)	Tyr353, Trp301, Tyr297, Thr316, Gly414
CNP0429848	−7.7	Asp320 (3.07), Ser346 (2.87), Glu348 (2.93), Trp301 (2.97)	Glu319, Thr349, Tyr297, Thr316
CNP0431416	−7.7	Thr413 (3.22), Asp320 (3.07)	Glu319, Gly318, Ser346, Trp301, Tyr353, Thr316, Tyr297
CNP0430001	−7.7	Trp301 (2.80)	Thr349, Tyr353, Tyr297, Asp320, Gly318, Thr316
CNP0425191	−7.7	Trp301 (2.91)	Tyr297, Pro317, Gly318, Glu319, Asp320, Thr413, Lys351, Tyr353, Thr316
CNP0430243	−7.7	Asp320 (3.11, 3.08)	Glu319, Thr316, Tyr353, Trp301, Tyr297
CNP0430629	−7.7	Asn300 (2.96), Trp301 (3.30)	Pro317, Thr316, Asp320, Tyr297, Glu348, Thr349, Tyr353
CNP0428673	−7.7	Asp320 (2.98)	Thr413, Lys351, Gly414, Tyr353, Thr316, Trp301, Tyr297, Gly318, Pro317, Glu319
CNP0436671	−7.7	Tyr353, Trp301	Asp320, Thr316, Tyr297, Ser298, Asn300, Glu348, Ser346, Thr349
CNP0426537	−7.7	Thr413 (3.32), Tyr353 (2.90, 3.08), Thr349 (2.98), Ser346 (3.06)	Trp301, Tyr297, Thr316, Asp320
CNP0424487	−7.7	Tyr353 (3.00, 2.85), Asn300 (3.24)	Tyr297, Thr349, Trp301, Glu348, Thr316, Asp320
CNP0435084	−7.6	Trp301 (3.02)	Asp320, Tyr353, Thr316, Tyr297
CNP0427078	−7.6	Asp320 (3.07)	Glu319, Tyr297, Tyr353, Trp301, Thr316, Pro317
CNP0428129	−7.6	Trp301 (2.95)	Asp320, Thr316, Tyr297, Thr349, Ser346
CNP0428690	−7.6	Trp301 (3.07)	Thr316, Thr349, Thr413, Asp320, Tyr297, Tyr353
CNP0426556	−7.6	Asp320 (2.85)	Glu319, Gly318, Tyr297, Trp301, Tyr353, Thr316, Glu319
CNP0434073	−7.6	Asp320 (3.09, 3.04)	Glu319, Tyr297, Thr349, Ser346, Trp301, Thr316, Tyr353
CNP0436112	−7.6	Asp320 (3.22)	Glu319, Pro317, Thr349, Ser346, Glu348, Tyr297, Thr316, Trp301, Tyr353, Gly318
CNP0432838	−7.6	Glu348 (3.05), Trp301 (3.03, 2.85), Ser346 (2.76)	Asn300, Thr349, Tyr297, Asp320, Glu319, Thr316, Pro317
CNP0436788	−7.6	Pro317 (2.86)	Glu319, Tyr297, Trp301, Thr316, Ser346, Tyr353, Thr413, Asp320
CNP0433836	−7.6	Asp320 (3.06), Thr413 (2.77), Tyr353 (2.79), Lys (2.99)	Tyr297, Thr316, Ser346, Gly414, Trp301
CNP0434686	−7.6	Asn300 (3.31, 2.81)	Glu348, Thr349, Ser346, Trp301 Asp320, Tyr297, Thr316 Tyr353
CNP0424603	−7.6	Trp301 (3.12), Tyr353 (2.70), Asp320 (3.05)	Glu319, Glu348, Ser346, Tyr297, Thr316
CNP0431117	−7.6	Tyr297 (3.10), Asn300 (2.85), Glu348 (3.01, 300), Trp301 (2.86)	Glu319, Gly318, Asp320, Thr316, Tyr353
CNP0433323	−7.6	Asp320 (3.06, 3.18)	Thr349, Tyr297, Trp301, Thr316, Tyr353, Gly318, Glu319
CNP0432515	−7.5	Trp301 (3.12), Glu348 (3.06)	Thr316, Tyr297, Asp320, Tyr353
CNP0434409	−7.5	Asn300 (3.23), Trp301 (2.96), Tyr297 (3.07)	Glu348, Thr349, Thr316, Tyr353
CNP0426246	−7.5	Ser346 (3.31)	Trp301, Thr349, Tyr297, Asp320, Glu319, Pro317, Thr316, Tyr353
CNP0436152	−7.5	Ser346 (2.95)	Thr349, Tyr297, Asp320, Thr316, Tyr353, Trp301
CNP0424683	−7.5	Trp301 (3.05), Asp320 (2.93)	Glu348, Ser346, Thr349, Tyr297, Glu319
CNP0434023	−7.5	Tyr353 (2.71)	Glu319, Asp320, Thr316, Tyr297, Trp301
CNP0428145	−7.5	Pro317 (3.25)	Asp320, Glu319, Tyr353, Thr316, Glu348, Trp301, Ser346, Tyr297
CNP0431895	−7.5	Ser346 (3.19), Tyr353 (3.05)	Tyr297, Asp320, Thr316, Trp301, Thr349, Lys351
CNP0424402	−7.5	Ile415 (3.30)	Tyr353, Asp320, Glu348, Thr349, Trp301, Ser346, Tyr297, Thr316
CNP0424427	−7.5	Trp301 (2.97)	Glu348, Tyr297, Asp320, Thr316, Tyr353
CNP0434660	−7.5	Asp320 (3.06)	Trp301, Thr316, Glu319, Gly318, Pro317, Tyr297, Tyr353

This was to analyze the common residues the ligands interact with for both complexes. This further validates AutoDock Vina's ability to predict the binding pose of a ligand in the binding pocket of a receptor.

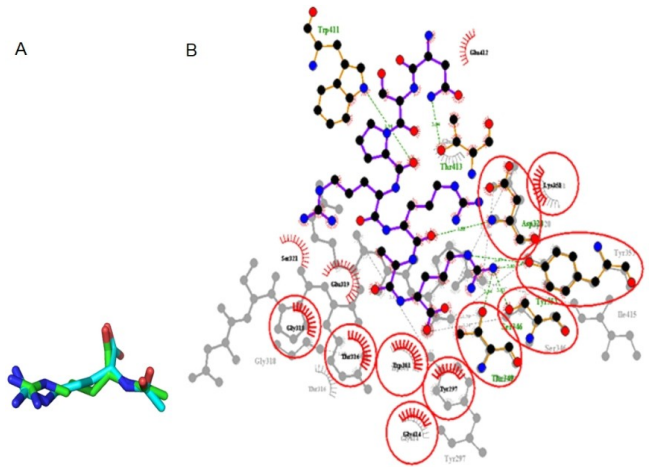

Figure 3. Aligning of the ligands of the co-crystallized complex (cyan) and the redocked complex (green) (A) The co-crystallized and redocked ligands align to determine the RMSD (B) The co-crystallized and redocked complexes superimposed in LigPlot + to identify the common interacting residues in both complexes.

Characterization of protein-ligand interaction

Hydrophobic and hydrogen bonding, which are crucial for ligand stability,[46] were employed to analyze the binding processes of the 34 hits. Out of the 34 hits, 20 interacted with at least one of these residues: Tyr297, Trp301, Thr316, Asp320, Ser346, Ther349 and Tyr353 (Table 1 and Figure 4). These 20 hits formed at least a hydrogen bond and several hydrophobic interactions. These residues are the active sites of NRP-1 hence an inhibitor of NRP-1 must interact with them.[15,30] In addition, Asp320 has also been shown to be a critical residue in the activity of NRP-1[37] (Figure 4). Therefore, compounds that interact with Asp320 might inhibit NRP-1. The C-end Rule interacted with Tyr297, Glu414, and Thr316 via hydrophobic interaction and hydrogen bond with Ser346, Thr349, Tyr353 and Asp320 (Figure S3). CNP0427474 formed hydrogen bonds Asp320 and Glu348 while forming hydrophobic interactions with Thr316, Tyr297, Trp301 and Tyr353. CNP0435132 formed hydrogen bond with Asp320 and hydrophobic interactions with Glu319, Pro317, Thr316, Trp301, Tyr297 and Tyr353. CNP0424372 formed hydrogen bond with Asp320 and hydrophobic interaction Gly414, Tyr297, Thr316, Tyr353 and Trp301. CNP0435311 interacted with Trp301 via hydrogen bond and hydrophobic interactions with Glu348, Thr349, Asp320, Thr316, Trp353 and Tyr297. CNP0429647 formed hydrogen bond with Trp301 and hydrophobic interactions with Tyr297, Gly414, Thr316, Asp320, Tyr353 and Thr413 (Table 1). All the potential leads interacted with Asp320, Thr316, Ser346 and Tyr353, implying their plausibility to inhibit the interaction between the C-end Rule and NRP-1.[47,48] Studies have shown that compounds that interact with these residues might hinder the interaction between the C-end Rule and the b1 subdomain of NRP-1 which might lead to its inhibition.[47]

Antiviral and BBB permeability prediction

NRP-1 is expressed by the brain cells.[49] It has also been established that SARS-CoV-2 permeates the BBB in order to get access to the brain.[10] It is imperative for NRP-1 inhibitors to permeate the BBB in order to inhibit the interaction between the C-end Rule and NRP-1.

COVID-19 is a viral disease hence drug candidates for COVID-19 must be antiviral.[50] Prediction for Activity for Substance Spectra (PASS) is an online server that utilizes Quantitative Structure-Activity Relationships (QSAR) of about 31,000 biologically active substances to predict the activity of small compounds.[51] Six hits were predicted to be both BBB permeate and antiviral with probability of active (Pa) values ranging from 0.414 to 0.779 (Table 2).

CNP0435132 and CNP0427474 belong to the class of compounds carboxylic acid renowned for their antiviral poten-

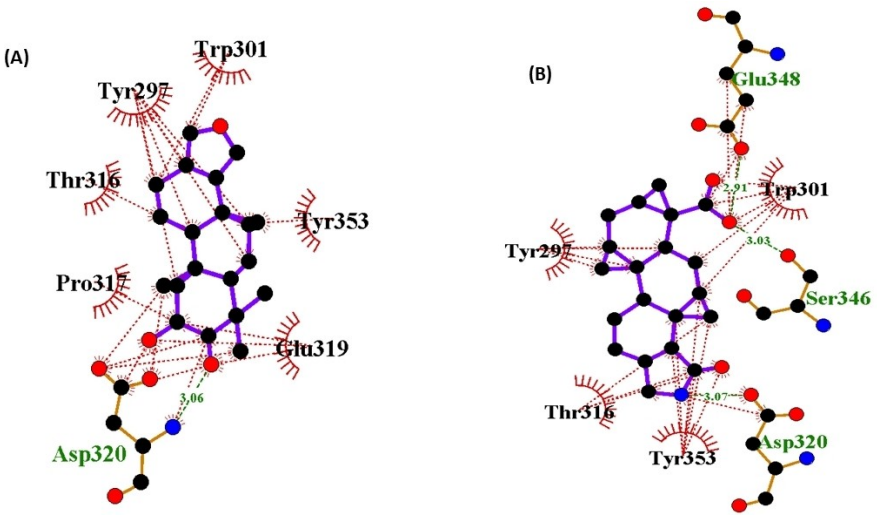

Figure 4. 2D of Protein-ligand interaction of illustrating the types of bonds formed between (A) CNP0435132 and (B) CNP0427474 and the b1 subdomain. Green dashes indicate hydrogen bond and red dashes indicate hydrophobic interactions.

Table 2. The 6 hits and 2D structure. Among the 20 compounds, these 6 were predicted to be antiviral and BBB permeate. The first 5 hits were selected for MD simulation.

Compound	BBB Permeation	Antiviral		2D Image
		Pa	Pi	
CNP0427474	Yes	0.779	0.003	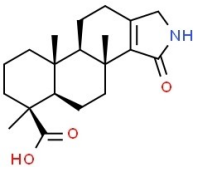
CNP0435132	Yes	0.750	0.004	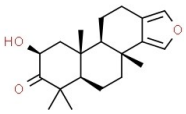
CNP0429647	Yes	0.668	0.008	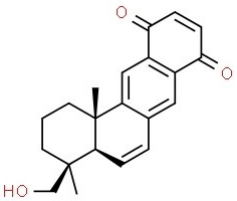
CNP0424372	Yes	0.414	0.077	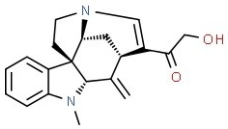
CNP0435311	Yes	0.470	0.009	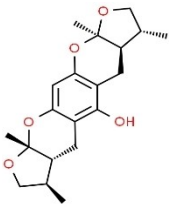
CNP0429190	Yes	0.663	0.008	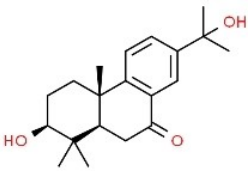

tial. An analog of CNP0435132 has demonstrated effectiveness against both RSV LONG and A2 strains, with IC_{50} values of 2.3 and 2.8 μM, respectively.[52] CNP0427474, characterized as a carboxylic acid and quinoline carboxylic derivative, has exhibited notable antiviral properties, with an EC_{50} value of 2 nM against VSV influenza.[53] Furthermore, CNP0427474 is structurally similar to vinorelbine, a therapeutic for influenza B. CNP0424372 is structurally similar to strychnine, an experimental drug for the central nervous system against convulsion. In addition, CNP0424372, an alkaloid, has demonstrated activity against the dengue virus, with an EC_{50} value of 8.8 μg/mol.[54] Furthermore, triterpenes such as CNP0435311 are well-recognized for their antiviral properties[55] with CNP0435311 being structurally similar to Phlorizin an active compound against measles virus.[56] CNP0429647, a derivative of anthraquinones have been reported to possess antiviral activity.[57]

Molecular dynamics (MD) simulation

The top 5 hits' complexes, the EG00229 complex, the C-end Rule complex and the unbound protein were subjected to a 200 ns MD simulation. MD simulation gives insight into the folding of the protein due to conformational changes with respect to time, utilizing Newton's laws of motion.[58–60] Root Mean Square Deviation (RMSD), Root Mean Square Fluctuation (RMSF), Radius of Gyration (Rg) and Hydrogen bond (H-bond) plots were computed. This was to identify scaffolds that manage to stay with the binding cleft and maintain steady

interaction with critical residues Asp320, Tyr353, Ser346, Tyr297 and Thr349.[61]

The RMSD time trajectory displays how a protein structure differs from a reference structure over time.[62] This gives an insight into stability as it undergoes conformational changes. The RMSD value of a residue typically represents the local flexibility of a protein. It represented an atom's mobility along the track of the simulation.[63,64] As a result, a larger residue RMSD value means that the mobility is higher, while a lower residue RMSD value means that the mobility is lower.[65,66] This then gives more insight into how the atoms of the protein and the complexes displace from the backbone.[67] The RMSD plot for the NRP-1 complexes and the unbound protein revealed that the complexes and the apo protein converged at about 8 ns (Figure 5). Subsequently, both the apo protein and the corresponding ligand complexes displayed a favorable stability throughout the simulation (Figure 5), with overall average values of 0.112, 0.121, 0.115, 0.119, 0.118, 0.122, 0.114, and 0.120 nm for apo-NRP-1, eg00229, C-end rule, CNP0427474, CNP0429647, CNP0424372, CNP0435311 and CNP0425132 respectively (Table S1). Previous studies where inhibitors of NRP-1 were identified reported a similar RMSD pattern, showing that the compounds stayed well bound to NRP-1 and formed stable complexes.[48,61,68]

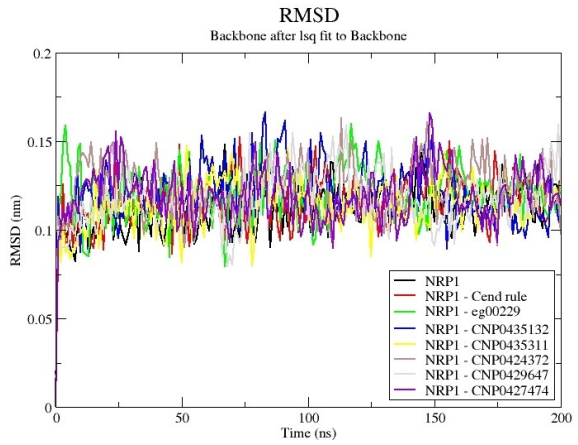

Figure 5. RMSD of the unbound protein (black) and the C-end Rule (red), EG00229 (green), CNP0435132 (blue), CNP0435311 (yellow), CNP0424372 (brown), CNP0429647 (grey) and CNP0427474 (violet) complexes.

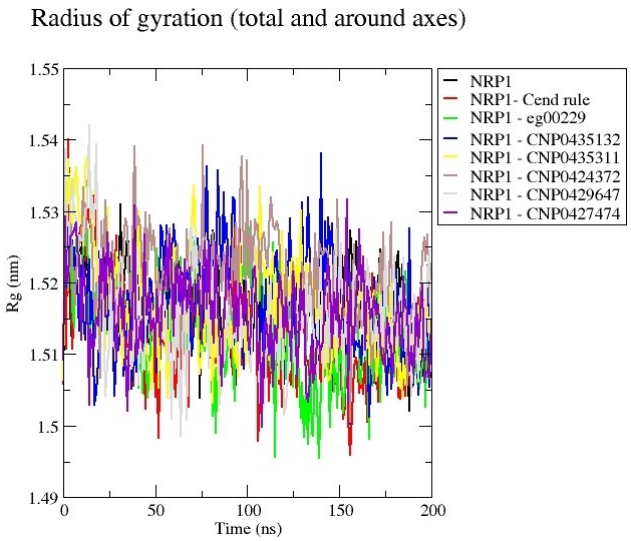

Figure 6. Radius of Gyration of the unbound protein (black) and the C-end Rule (red), EG00229 (green), CNP0435132 (blue), CNP0435311 (yellow), CNP0424372 (brown), CNP0429647 (grey) and CNP0427474 (violet) complexes.

Rg gives insight about the compactness of a macromolecule hence determining the folding of the macromolecule.[69–71] The change of the Rg over time (Figure 6) indicates the unfolding of a protein and a stable Rg depicts compactness and folding.[72] For all the complexes and the unbound protein, a stable Rg was observed ranging from 1.513 to 1.521 nm (Table S1). Overall, an average Rg of about 1.516 nm was observed corroborating an earlier study where an average Rg of 1.511 nm was obtained, suggesting compactness upon ligand binding.[61,73]

Analysis of RMSF determines the volatility of the residues of the protein.[74] Residues with less fluctuation indicate that those residues are involved in binding.[75] The RMSF of all the complexes and unbound protein was similar with fewer fluctuations at the active site residues (Figure 7) as indicated by Sabki et al, 2023. This corroborates results from previous studies where the b1 subdomain has been shown to be suitable for ligand binding.[29]

Analysis of hydrogen bonds is essential for predicting the protein-ligand complex's stability. The stability of the protein-ligand complex increases with the amount of intermolecular hydrogen bonds.[76] The number of hydrogen bonds established throughout the simulation was evaluated to assess the interactions between the NRP-1 and the ligands. CNP0435132 formed a maximum of 4 hydrogen bonds and an average of 3 hydrogen bonds throughout the simulation time. CNP0427474 formed a maximum of 3 hydrogen bonds and an average of 1 hydrogen bond. CNP0435311, CNP0424372 and CNP0429647 formed a maximum of 2 hydrogen bonds and an average of 1 hydrogen bond (Figure 8). This implies that continuous interactions formed between the binding sites and the potential.[77]

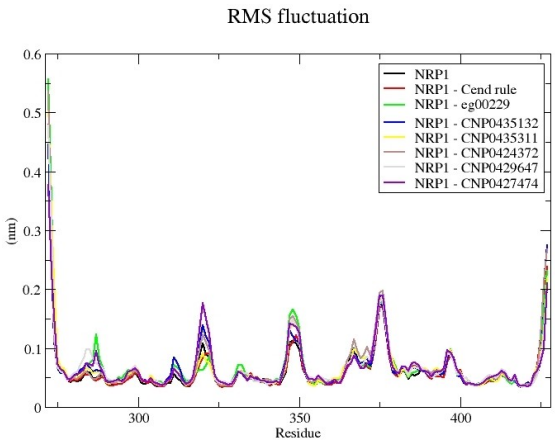

Figure 7. RMSF of the unbound protein (black) and the C-end Rule (red), EG00229 (green), CNP0435132 (blue), CNP0435311 (yellow), CNP0424372 (brown), CNP0429647 (grey) and CNP0427474 (violet) complexes.

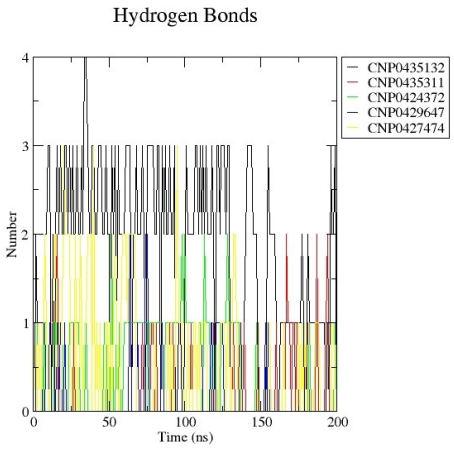

Figure 8. Hydrogen bonds formed over the simulation time CNP0435132 (blue), CNP0435311 (yellow), CNP0424372 (brown), CNP0429647 (grey) and CNP0427474 (violet) complexes.

The protein surface's exposure to solvent molecules is measured by the Solvent Accessible Surface Area (SASA). By analyzing the impact of the solvent environment, it may provide insight into the molecule's stability and compactness. The more exposed the proteins' hydrophobic amino acid residues are, the lower the SASA value, and the more stable the system is.[61,66,77,78] Average SASA values ranging from 86.433 to 89.410 nm^2 (Table S1) were observed with the NRP-1-Cend Rule complex displaying the highest SASA value of 89.410 nm^2 suggesting more protein compactness and stability upon ligand binding (Figure S1).

Molecular mechanics-Poisson Boltzmann surface area (MM-PBSA) calculation

Molecular mechanics-Poisson Boltzmann surface area (MM/PBSA) is a widely used approach to determine the binding free energy between a ligand and a macromolecule.[79] It has been shown that simulation-based binding affinities are more precise than computational-based binding affinities such as molecular docking.[79,80] The binding free energies of 7 protein-ligand complexes were computed. The results obtained had a similar trend to AutoDock Vina's results. NRP-1 inhibitor, EG00229 had a higher binding affinity than the C-end Rule. This has also been observed in previous studies where EG00229 had a higher binding affinity to NRP-1 than the C-end Rule.[36] The 5 potential leads had higher binding affinity to NRP-1 than both the C-end Rule and EG00229 (Table 3). This corroborates the results from the docking. High binding affinity indicates a high plausibility of inhibition[81] hence, the potential leads are plausible inhibitors of the interaction between NRP-1 and the C-end Rule.

To further validate the MM-PBSA and the docking results, PRODIGY web server[82,83] was employed. The last 5 ns frame of the MD simulations of the C-end Rule and the 5 potential leads were extracted, and their binding energies were estimated. C-end Rule, CNP0435132, CNP0435311, CNP0424372, CNP0429647 and CNP0427474 had average binding energies of −5.9, −7.1, −6.0, −6.4, −6.6 and −6.0 kcal/mol respectively.

Energy decomposition per residue is a measure of the energy each residue in a protein-ligand complex contributes to ligand interaction with a receptor.[84] Residues that contribute energy less than −5 kJ/mol or greater than 5 kJ/mol have been reported to be critical residues in the ligand interaction with a receptor.[85] For the NRP-1-CNP0435132 complex, Asp320 contributed 5.8 kJ/mol, implying its crucial role in ligand binding to NRP-1 (Figure S2). This corroborates earlier studies where Asp320 was reported as a critical residue in the ligand binding of NRP-1.[86]

Conclusions

In this study, we harnessed virtual screening to pinpoint potential inhibitors of NRP-1, an emerging target exploited by SARS-CoV-2 for neural system entry. Our meticulous examination of 1930 drug-like compounds, in accordance with Lipinski's Rule of Five, led us to identify five novel potential leads: CNP0435132, CNP0435311, CNP0424372, CNP0429647, and CNP0427474. These compounds exhibited promising binding energies; −8.2, −8.1, −10.7, −8.2, −8.2 kcal/mol, respectively and displayed interactions with critical residues Asp320, Tyr297, Ser346, Thr349, and Tyr353. An in-depth exploration of their pharmacokinetic properties revealed permeability through the blood-brain barrier, along with potential antiviral activity, as indicated by probable active values ranging from 0.414 to 0.779. MD simulation and MM-PBSA calculation further bolstered our findings, confirming the stability and compactness of

Table 3. The average energy terms of the 5 potential leads, C-end Rule and Eg00229 with their deviation in kJ/mol.

Compound	van der Waals energy [kJ/mol]	Electrostatic energy [kJ/mol]	Polar solvation energy [kJ/mol]	Nonpolar energy [kJ/mol]	Binding energy [kJ/mol]
C-end-rule	−38.600 ± 3.960	−138.164 ± 15.785	241.250 ± 23.213	−6.833 ± 0.691	58.334 ± 3.504
eg00229	−52.658 ± 2.909	−173.506 ± 9.949	256.231 ± 12.598	−8.524 ± 0.445	21.697 ± 2.645
CNP0435132	−41.784 ± 2.574	−35.633 ± 2.919	59.026 ± 4.823	−6.350 ± 0.410	−24.598 ± 2.406
CNP0435311	−30. 019 ± 2.162	−3.536 ± 0.477	15.513 ± 2.529	−4.272 ± 0.303	−22. 381 ± 2.389
CNP0424372	−50.852 ± 2.431	−15.728 ± 1.091	47.603 ± 3.175	−7.054 ± 0.321	−25.789 ± 1.957
CNP0429647	−29.677 ± 2.434	−2.807 ± 0.608	12.913 ± 2.767	−3.939 ± 0.299	−23.664 ± 2.962
CNP0427474	−39.678 ± 2.427	−9.582 ± 1.016	34.211 ± 3.079	−5.647 ± 0.335	−20.611 ± 2.368

the complexes formed between these natural compounds and NRP-1, consistent with earlier studies.

In conclusion, these natural compounds can therefore be experimentally be investigated and could serve as promising scaffolds for the development of NRP-1 inhibitors, holding significant potential for therapeutic interventions aimed at mitigating the neuroinfectivity associated with SARS-CoV-2.

Methods

Target Retrieval and Preparation

An exhaustive search was conducted at the Research Collaboratory for Structural Bioinformatics (RCSB) Protein Data Bank (PDB).[87] Twenty-four structures of NRP-1 were found. The 3D X-ray crystallographic structure of NRP-1 in a complex with the C-end rule (PBD ID: 7JJC) was selected for this study. The protein was viewed using PyMOL (PyMOL Molecular Graphics System, Version 2.5.0, Schrödinger, LLC) GROningen MAchine for Chemical Simulations (GROMACS) version 2018.8[88] was used to minimize the energy of the protein. This was done by creating a topology file of the structure which contains all required information such as atom masses, bond length, and angles was created at a reasonable force field (Optimized Potentials for Liquid Simulations (OPLS)/All Atom (AA) force field)[89].

Small Molecules Retrieval and Preparations

An integrated library of 1930 compounds from the COCONUT (COlleCtion of Open NatUral ProducTs) database[90] that do not violate both Lipinski's rule of five (RO5)[91] and Veber rule[92] and are predicted to be non-toxic, two known inhibitors of NRP1, EG01377 and EG00229 and Cend Rule of the spike protein of SARS-CoV-2 were employed for this study. An Open Babel 2.4.0[93] was used to convert the structure data file (sdf) format of the 1930 compounds into AutoDock files format (pdbqt). Prior to the conversion, the energies of the compounds were minimized using the Universal Force Field (UFF).[94]

Molecular Docking

AutoDock Vina 1.1.2[95] was employed for the molecular docking. A grid box of dimensions 21.374, 28.274 and 23.5115 $Å^3$ centered at 23.367, 43.539 and 40.982 Å in accordance with the x, y, and z coordinates (around the b1 subdomain) was used. AutoDock Vina's threshold of −7.0 kcal/mol can discriminate between putative specific and non-specific protein-ligand bonds[96] hence a more stringent threshold of −8.0 kcal/mol was utilized to identify compounds with higher binding affinity to NRP-1. Compounds with binding energies higher than −8.0 kcal/mol were not selected. PyMOL version 2.5.0 was used to visually inspect the results to select the best docked ligands.

Assessment of Docking Protocol

LigAlign[43] was used to validate the docking protocol. The ligand co-crystallized structure of NRP-1 was removed and redocked. The co-crystallized complex and the redocked complex were superimposed with LigAlign to determine the Root Mean Square Deviation (RMSD) between the ligand of the co-crystallized structure and the redocked structure. The co-crystallized and the re-docked complex were then superimposed using LigPlot + version 1.4.5.[97]

Protein-Ligand Interaction Characterization

The protein-ligand interaction of the complexes was analyzed using LigPlot + version 1.4.5.[97] The 2D protein-ligand interactions generated showed hydrogen bonds and hydrophobic interactions. The best pose of the hits was saved in ".pdb" file format and visualized in PyMOL (PyMOL Molecular Graphics System, Version 2.5.0, Schrödinger, LLC) before serving the complexes as input for LigPlot +. The hydrogen bonds were denoted as green dashed lines and the arcs with spokes radiating towards the ligands as hydrophobic interactions.

Antiviral and BBB Permeability Prediction

The antiviral activity of the hits was determined using Prediction of Activity Spectra for Substances (PASS).[51] The Simplified Molecular Input Line-Entry System (SMILES) format of the compounds served as inputs. The structural-activity link between the compound of interest and a training set of over 31,000 compounds with known biological activities is used by PASS to determine the relevant biological activities of compounds. PASS predicts the probability of active (Pa) and probability of inactive (Pi) for each given chemical, with both values ranging between 0.000 and 1.000 for a predicted activity. When the Pa is more than the Pi for a chemical activity and Pa $>$ 0.3, the pharmacological activity should be investigated.[98,99] The BBB permeation of the hits was determined by SwissADME,[100] an online tool to evaluate the pharmacokinetic properties and druglikeness of a compound.

Molecular Dynamics Simulation and Molecular Mechanics-Poisson Boltzmann Surface Area (MM-PBSA) Calculations

The unbound protein and 7 protein-ligand complexes were subjected to a 200 ns Molecular Dynamics (MD) simulation using GROningen Machine for Chemical Simulation (GROMACS) 2018 version.[88] The ligands' topology was generated by employing SwissParam[101] while CHARMM 27 all atoms force field was used to generate the topology of the protein after which the system was placed in cubic simulation box with a distance of 1 nm from the edges. Ions of concentration 0.15 M were added to neutralize the system before the energy of the system was minimized for 5,000 nsteps for relaxation. The

system was then equilibrated at a temperature of 300 K and density of 1,020 kg/m^3 for nsteps of 5,000. Xmgrace version 5.1.11 was used to analyze the results. Finally, the grid box size and center were set exactly the same for NRP-1 and the complexes.[64]

Molecular Mechanics-Poisson Boltzmann surface Area (MM-PBSA) calculations were carried out to determine the binding free energy (△G) of the complexes using g-mmpbsa,[102] a tool for high-throughput MM-PBSA calculations. The free binding energy (△G) was calculated using the equation below.

$$\Delta G_{MM-PBSA} = \Delta G_{complex} - (\Delta G_{protein} + \Delta G_{ligand})$$

Author Contributions

M. A., L.A and J.S. designed, analyzed, and wrote the original article draft. L.A., C.A., S.M., M.M.B. and D.O.Y. reviewed the final article. All authors read and approved the manuscript.

Acknowledgements

The High-Performance Computing System, Zuputo at the University of Ghana, West Africa Center for Cell Biology of Infectious Pathogens (WACCBIP).

Conflict of Interests

The authors declare no conflict of interest.

Data Availability Statement

The data that support the findings of this study are available from the corresponding author upon reasonable request.

Keywords: C-end rule · molecular docking · molecular dynamics · neuropilin-1 · SARS-CoV-2

[1] S. Baloch, M. A. Baloch, T. Zheng, X. Pei, *Tohoku J. Exp. Med.* **2020**, *250*, 271–278.
[2] S. Muralidar, S. V. Ambi, S. Sekaran, U. M. Krishnan, *Biochimie.* **2020**, *179*, 85–100.
[3] S. K. Kwofie, E. Broni, S. O. Asiedu, G. B. Kwarko, B. Dankwa, K. S. Enninful, *Molecules.* **2021**, *26*.
[4] W. H. O. 2023.
[5] B. Hu, H. Guo, P. Zhou, Z. L. Shi, *Nat. Rev. Microbiol.* **2021**, *19*, 141–154.
[6] A. Gupta, M. V. Madhavan, K. Sehgal, N. Nair, S. Mahajan, T. S. Sehrawat, *Nat. Med.* **2020**, *26*, 1017–1032.
[7] A. Kumar, V. Pareek, P. Prasoon, M. A. Faiq, P. Kumar, C. Kumari, *J. Neurosci. Res.* **2020**, *98*, 2376–2383.
[8] C. K. Bullen, *Altex.* **2020**, *37*, 665–671.
[9] A. Kumar, V. Pareek, P. Prasoon, M. A. Faiq, P. Kumar, C. Kumari, *J. Neurosci. Res.* **2020**, *98*, 2376–2383.
[10] S. Krasemann, U. Haferkamp, S. Pfefferle, M. S. Woo, F. Heinrich, M. Schweizer, *Stem Cell Reports* **2022**, *17*, 307–320.
[11] L. Cantuti-Castelvetri, R. Ojha, L. D. Pedro, M. Djannatian, J. Franz, S. Kuivanen, *Science.* **2020**, *370*, 856–860.
[12] J. L. Daly, B. Simonetti, K. Klein, K. E. Chen, M. K. Williamson, C. Antón-Plágaro, D. K. Shoemark, L. Simon-Garcia, M. Bauer, R. Hollandi, U. F. Greber, P. Horvath, R. B. Sessions, A. Helenius, J. A. Hiscox, T. Teesalu, D. A. Matthews, A. D. Davidson, B. M. Collins, P. J. Cullen, Y. Yamauchi, *Science* **2020**, *370*, 861-865.
[13] A. Kumar, R. K. Narayan, P. Prasoon, C. Kumari, G. Kaur, S. Kumar, *Front. Immunol.* **2021**, *12*.
[14] B. S. Mayi, J. A. Leibowitz, A. T. Woods, K. A. Ammon, A. E. Liu, A. Raja, *PLoS Pathog.* **2021**, *17*, 1–8.
[15] Y. Şimşek, S. S. Baran, B. Aslım, *J. Mol. Graphics Modell.* **2021**, *109*.
[16] H. F. Guo, C. W. V. Kooi, *J. Biol. Chem.* **2015**, *290*, 29120–29126.
[17] X. Li, M. W. Parker, C. W. K. V. Kooi, *Biomol. Concepts* **2014**, *5*, 157–166.
[18] S. D. Liu, L. P. Zhong, J. He, Y. X. Zhao, *Chin. Med. J. (Engl. Ed.)* **2021**, *134*, 508–517.
[19] F. Mota, C. Fotinou, R. R. Rana, A. W. E. Chan, T. Yelland, M. T. Arooz, *FEBS J.* **2018**, *285*, 1290–1304.
[20] E. C. Abebe, T. M. Ayele, Z. T. Muche, T. A. Dejenie, *Biologics* **2021**, *15*, 143–152.
[21] S. D. Liu, L. P. Zhong, J. He, Y. X. Zhao, *Chin. Med. J. (Engl. Ed.)* **2021**, *134*, 508–517.
[22] C. Raimondi, C. Ruhrberg, *Semin. Cell Dev. Biol.* **2013**, *24*, 172–178.
[23] B. A. Appleton, P. Wu, J. Maloney, J. P. Yin, W. C. Liang, S. Stawicki, *EMBO J.* **2007**, *26*, 4902–4912.
[24] S. Satarker, M. Nampoothiri, *Arch. Med. Res.* **2020**, *51*, 482–491.
[25] J. Shang, Y. Wan, C. Luo, G. Ye, Q. Geng, A. Auerbach, *Proc. Nat. Acad. Sci.* **2020**, *117*.
[26] Y. Huang, C. Yang, X. X. Feng, W. Xu, S. W. Liu, *Acta Pharmacol. Sin.* **2020**, *41*, 1141–1149.
[27] D. Bestle, M. R. Heindl, H. Limburg, T. van Lam, O. Pilgram, H. Moulton, *Life Sci. Alliance* **2020**, *3*, 1–14.
[28] A. Jobe, R. Vijayan, *Comput. Struct. Biotechnol. J.* **2021**, *19*, 1889–1895.
[29] F. Mota, C. Fotinou, R. R. Rana, A. W. E. Chan, T. Yelland, M. T. Arooz, *FEBS J.* **2018**, *285*, 1290–1304.
[30] A. Jarvis, C. K. Allerston, H. Jia, B. Herzog, A. Garza-Garcia, N. Winfield, *J. Med. Chem.* **2010**, *53*, 2215–2226.
[31] S. Perez-Miller, M. Patek, A. Moutal, P. Duran, C. R. Cabel, C. A. Thorne, S. K. Campos, R. Khanna, *ACS Chem. Neurosci.* **2021**, *12*, 1299–1312.
[32] A. A. Siddiqui, F. Iram, S. Siddiqui, K. Sahu, *Int. J. Drug Dev. Res.* **2014**, *6*, 172–204.
[33] P. M. Cheuka, G. Mayoka, P. Mutai, K. Chibale, *Molecules.* **2017**, *22*.
[34] I. Chandra, C. Nayak, S. K. Singh, in *Innov. Implementations Comput. Aided Drug Discov. Strateg. Ration. Drug Des.*, Springer Singapore, Singapore, **2021**, pp. 153–177.
[35] D. S. N. B. K. Prasanth, M. Murahari, V. Chandramohan, S. P. Panda, L. R. Atmakuri, C. Guntupalli, *J. Biomol. Struct. Dyn.* **2021**, *39*, 4618–4632.
[36] M. Klaewkla, T. Charoenwongpaiboon, P. Mahalapbutr, *J. Mol. Liq.* **2021**, 335–116537.
[37] J. L. Vique-Sánchez, *Bioorg. Med. Chem.* **2021**, *33*, 116040.
[38] S. Perez-Miller, M. Patek, A. Moutal, P. Duran, C. R. Cabel, C. A. Thorne, S. K. Campos, R. Khanna, *ACS Chem. Neurosci.* **2021**, *12*, 1299–1312.
[39] M. W. Chang, W. Lindstrom, A. J. Olson, R. K. Belew, *J. Chem. Inf. Model.* **2007**, *47*, 1258–1262.
[40] A. I. Trujillo-Correa, D. C. Quintero-Gil, F. Diaz-Castillo, W. Quiñones, S. M. Robledo, M. Martinez-Gutierrez, *BMC Complementary Altern. Med.* **2019**, *19*, 298.
[41] S. Ahmad, Y. Waheed, A. Abro, S. W. Abbasi, S. Ismail, *J. Mol. Model.* **2021**, *27*, 206.
[42] R. Škrbić, M. Travar, M. P. Stojiljković, D. M. Djuric, R. Suručić, *Molecules.* **2023**, *28*.
[43] A. Heifets, R. H. Lilien, *J. Mol. Graphics Modell.* **2010**, *29*, 93–101.
[44] B. P. Brown, J. Mendenhall, J. Meiler, *J. Chem. Inf. Model.* **2019**, *59*, 689–701.
[45] M. J. Alves, H. J. C. Froufe, A. F. T. Costa, A. F. Santos, L. G. Oliveira, S. R. M. Osório, *Molecules.* **2014**, *19*, 1672–1684.
[46] S. K. Kwofie, S. O. Asiedu, R. Koranteng, E. Quarshie, E. K. Tiburu, W. A. Miller, *Inf. Med. Unlocked* **2022**, *30*, 100957.
[47] A. Kolarič, M. Jukič, U. Bren, *Pharmaceuticals.* **2022**, *15*, 165.
[48] R. Škrbić, M. Travar, M. P. Stojiljković, D. M. Djuric, R. Suručić, *Molecules.* **2023**, *28*.
[49] J. Davies, H. S. Randeva, K. Chatha, M. Hall, D. A. Spandidos, E. Karteris, *Mol. Med.* **2020**, *22*, 4221–4226.
[50] S. Kausar, F. Said Khan, M. Ishaq Mujeeb Ur Rehman, M. Akram, M. Riaz, G. Rasool, A. Hamid Khan, I. Saleem, S. Shamim, A. Malik, *Int. J. Immunopathol. Pharmacol.* **2021**, *35*, 20587384211002620.
[51] D. A. Filimonov, A. A. Lagunin, T. A. Gloriozova, A. V. Rudik, D. S. Druzhilovskii, P. V. Pogodin, *Chem. Heterocycl. Compd.* **2014**, *50*, 444–457.

[52] Y. Miao, Y. Hu, J. Yang, T. Liu, J. Sun, X. Wang, *RSC Adv.* **2019**, *9*, 27510–27540.
[53] P. Das, X. Deng, L. Zhang, M. G. Roth, B. M. A. Fontoura, M. A. Phillips, *ACS Med. Chem. Lett.* **2013**, *4*, 517–521.
[54] S. Faisal, S. L. Badshah, B. Kubra, A. H. Emwas, M. Jaremko, *Nat. Prod. Bioprospect.* **2023**, *13*, 4.
[55] A. M. Madureira, J. R. Ascenso, L. Valdeira, A. Duarte, J. P. Frade, G. Freitas, *Nat. Prod. Res.* **2003**, *17*, 375–380.
[56] E. Norrby, *Arch die gesamte Virusforsch.* **1966**, *18*, 333–343.
[57] F. Zhao, S. Zhao, J. T. Han, Y. F. Wang, Y. N. Wang, C. H. Wang, *Phytochem. Lett.* **2015**, *11*, 57–60.
[58] M. De Vivo, M. Masetti, G. Bottegoni, A. Cavalli, *J. Med. Chem.* **2016**, *59*, 4035–4061.
[59] X. Liu, D. Shi, S. Zhou, H. Liu, H. Liu, X. Yao, *Expert Opin. Drug Discovery* **2018**, *13*, 23–37.
[60] S. A. Hollingsworth, R. O. Dror, *Neuron.* **2018**, *99*, 1129–1143.
[61] A. Sabki, L. Khelifi, A. Kameli, S. Baali, *Chem. Biodiversity* **2023**, *20*, 3.
[62] X. Cheng, I. Ivanov, *Mol. Dyn.*. **2012**, *929*.
[63] A. Cetin, *Curr. Comput.-Aided Drug Des.* **2022**, *18*, 337–346.
[64] A. Cetin, *Chem. Phys. Lett.* **2021**, *771*, 138563.
[65] Y. Fu, J. Zhao, Z. Chen, *Comput. Math. Methods Med.* **2018**, *2018*.
[66] J. O. O. Uhomoibhi, F. O. Shode, K. A. Idowu, S. Sabiu, *J. Mol. Graphics Modell.* **2022**, *114*, 108185.
[67] K. Sargsyan, C. Grauffel, C. Lim, *J. Chem. Theory Comput.* **2017**, *13*, 1518–1524.
[68] E. Alshawaf, M. M. Hammad, S. K. Marafie, H. Ali, F. Al-Mulla, J. Abubaker, *Microb. Pathog.* **2022**, *170*, 105701.
[69] M. Y. Lobanov, N. S. Bogatyreva, O. V. Galzitskaya, *Mol. Biol.* **2008**, *42*, 623–628.
[70] A. K. Verma, S. F. Ahmed, M. S. Hossain, A. A. Bhojiya, A. Mathur, S. K. Upadhyay, *J. Biomol. Struct. Dyn.* **2021**, 1–17.
[71] Z. Jiang, L. You, W. Dou, T. Sun, P. Xu, *Polymers (Basel).* **2019**, *11*, 1–13.
[72] B. Dankwa, E. Broni, K. S. Enninful, S. K. Kwofie, M. D. Wilson, *Struct. Chem.* **2022**.
[73] P. O. Sakyi, E. Broni, R. K. Amewu, W. A. Miller, M. D. Wilson, S. K. Kwofie, *Front. Cell. Infect. Microbiol.* **2022**, *12*.
[74] Y. W. Dong, M. L. Liao, X. L. Meng, G. N. Somero, *Proc. Natl. Acad. Sci. USA* **2018**, *115*, 1274–1279.
[75] S. Sinha, S. M. Wang, *Comput. Struct. Biotechnol. J.* **2020**, *18*, 723–736.
[76] I. Baruah, G. Borgohain, *J. Mol. Graphics Modell.* **2022**, *111*.
[77] L. Adams, A. R. Issahaku, C. Agoni, M. Afiadenyo, K. Asamoah Kusi, S. Moane, D. Obiri-Yeboah, M. McKeon-Bennett, *Inf. Med. Unlocked* **2023**, *41*, 101319.
[78] S. A. Saah, P. O. Sakyi, D. Adu-Poku, N. O. Boadi, G. Djan, D. Amponsah, R. N. O. A. Devine, K. Ayittey, *J. Chem.* **2023**, *2023*, 1–20.
[79] C. Wang, P. H. Nguyen, K. Pham, D. Huynh, T. N. Le, H. Wang, P. Ren, R. Luo, **2017**, *37*, 2436–2446.
[80] E. Wang, H. Sun, J. Wang, Z. Wang, H. Liu, J. Z. H. Zhang, *Chem. Rev.* **2019**, *119*, 9478–9508.
[81] H. Yang, X. Li, G. Li, H. Huang, W. Yang, X. Jiang, *Biomed. Pharmacother.* **2021**, *139*, 111664.
[82] A. Vangone, J. Schaarschmidt, P. Koukos, C. Geng, N. Citro, M. E. Trellet, A. Valencia, *Bioinformatics.* **2001**, *35*, 1585–1587.
[83] A. Vangone, A. M. J. J. Bonvin, *eLife* **2015**, *4*, 1–15.
[84] N. Chaudhary, P. Aparoy, *Heliyon.* **2020**, *6*, e04944.
[85] E. Broni, C. Ashley, J. Adams, H. Manu, E. Aikins, M. Okom, *Int. J. Mol. Sci.* **2023**, *24*, 6298.
[86] J. L. Vique-Sánchez, *Bioorg. Med. Chem.* **2021**, *33*, 116040.
[87] S. Burley, C. Bhikadiya, C. Bi, S. Bittrich, L. Chen, G. V. Crichlow, *Nucleic Acids Res.* **2021**, *49*, 437–451.
[88] M. J. Abraham, T. Murtola, R. Schulz, S. Páll, J. C. Smith, B. Hess, *SoftwareX.* **2015**, *1–2*, 19–25.
[89] B. Doherty, X. Zhong, S. Gathiaka, B. Li, O. Acevedo, *J. Chem. Theory Comput.* **2017**, *13*, 6131–6145.
[90] M. Sorokina, P. Merseburger, K. Rajan, M. A. Yirik, C. Steinbeck, *J Cheminform.* **2021**, *13*, 1–13.
[91] C. A. Lipinski, F. Lombardo, B. W. Dominy, P. J. Feeney, *Adv. Drug Delivery Rev.* **2012**, *64*, 4–17.
[92] D. F. Veber, S. R. Johnson, H. Y. Cheng, B. R. Smith, K. W. Ward, K. D. Kopple, *J. Med. Chem.* **2002**, *45*, 2615–2623.
[93] N. M. O'Boyle, M. Banck, C. A. James, C. Morley, T. Vandermeersch, G. R. Hutchison, *J. Cheminf.* **2011**, *3*, 33.
[94] L. Jaillet, S. Artemova, S. Redon, *J. Mol. Graphics Modell.* **2017**, *77*, 350–362.
[95] O. Trott, A. J. Olson, *J. Comput. Chem.* **2009**, *31*.
[96] T. Pantsar, A. Poso, *Molecules.* **2018**, *23*, 1899.
[97] R. A. Laskowski, M. B. Swindells, *J. Chem. Inf. Model.* **2011**, *51*, 2778–2786.
[98] A. Lagunin, A. Stepanchikova, D. Filimonov, V. Poroikov, *Bioinformatics.* **2000**, *16*, 747–748.
[99] E. Broni, S. K. Kwofie, S. O. Asiedu, W. A. Miller, M. D. Wilson, *Biomol. Eng.* **2021**, *11*, 1–32.
[100] A. Daina, O. Michielin, V. Zoete, *Sci. Rep.* **2017**, *7*, 1–13.
[101] V. Zoete, M. A. Cuendet, A. Grosdidier, O. Michielin, *J. Comput. Chem.* **2011**, *32*, 2359–2368.
[102] R. Kumari, R. Kumar, A. Lynn, *J. Chem. Inf. Model.* **2014**, *54*, 1951–1962.

Manuscript received: August 14, 2023
Accepted manuscript online: October 25, 2023
Version of record online: ■■, ■■